AIP | Review of Scientific Instruments

Development of a mirror-based endoscope for divertor spectroscopy on JET with the new ITER-like wall (invited)

A. Huber, S. Brezinsek, Ph. Mertens, B. Schweer, G. Sergienko et al.

Citation: Rev. Sci. Instrum. **83**, 10D511 (2012); doi: 10.1063/1.4731759
View online: http://dx.doi.org/10.1063/1.4731759
View Table of Contents: http://rsi.aip.org/resource/1/RSINAK/v83/i10
Published by the American Institute of Physics.

Development of a mirror-based endoscope for divertor spectroscopy on JET with the new ITER-like wall (invited)[a)]

A. Huber,[1,b),c)] S. Brezinsek,[1,c)] Ph. Mertens,[1,c)] B. Schweer,[1,c)] G. Sergienko,[1,c)] A. Terra,[1,c)] G. Arnoux,[2] N. Balshaw,[2] M. Clever,[1,c)] T. Edlingdon,[2] S. Egner,[3] J. Farthing,[2] M. Hartl,[3] L. Horton,[4] D. Kampf,[3] J. Klammer,[5] H. T. Lambertz,[1,c)] G. F. Matthews,[2] C. Morlock,[4] A. Murari,[4] M. Reindl,[5] V. Riccardo,[2] U. Samm,[1,c)] S. Sanders,[2] M. Stamp,[2] J. Williams,[2] K. D. Zastrow,[2] C. Zauner,[5] and JET-EFDA Contributors[d)]

JET-EFDA, Culham Science Centre, Abingdon, OX14 3DB, United Kingdom

[1]*Institute of Energy and Climate Research – Plasma Physics, Forschungszentrum Jülich, EURATOM Association, Trilateral Euregio Cluster, D-52425 Jülich, Germany*

[2]*Euratom/CCFE Fusion Association, Culham Science Centre, Abingdon, OX14 3DB, United Kingdom*

[3]*Kayser-Threde GmbH, D-81379 Munich, Germany*

[4]*EFDA-JET Close Support Unit, Culham Science Centre, Culham, OX14 3DB, United Kingdom*

[5]*KRP-Mechatec Engineering GbR, D-85748 Garching b. Muenchen, Germany*

(Presented 7 May 2012; received 5 May 2012; accepted 6 June 2012; published online 11 July 2012)

A new endoscope with optimised divertor view has been developed in order to survey and monitor the emission of specific impurities such as tungsten and the remaining carbon as well as beryllium in the tungsten divertor of JET after the implementation of the ITER-like wall in 2011. The endoscope is a prototype for testing an ITER relevant design concept based on reflective optics only. It may be subject to high neutron fluxes as expected in ITER. The operating wavelength range, from 390 nm to 2500 nm, allows the measurements of the emission of all expected impurities (*W I*, *Be II*, *C I*, *C II*, *C III*) with high optical transmittance ($\geq$30% in the designed wavelength range) as well as high spatial resolution that is $\leq$2 mm at the object plane and $\leq$3 mm for the full depth of field ($\pm$0.7 m). The new optical design includes options for *in situ* calibration of the endoscope transmittance during the experimental campaign, which allows the continuous tracing of possible transmittance degradation with time due to impurity deposition and erosion by fast neutral particles. In parallel to the new optical design, a new type of possibly ITER relevant shutter system based on pneumatic techniques has been developed and integrated into the endoscope head. The endoscope is equipped with four digital CCD cameras, each combined with two filter wheels for narrow band interference and neutral density filters. Additionally, two protection cameras in the $\lambda > 0.95$ μm range have been integrated in the optical design for the real time wall protection during the plasma operation of JET.
 [http://dx.doi.org/10.1063/1.4731759]

I. INTRODUCTION

The installation of the ITER-like wall (ILW) (Ref. 1) in 2010–2011, namely, of the full beryllium first wall and of the tungsten divertor, is one the largest upgrades in the history of JET. This absolutely new material combination aims on the one hand at proving the usability of Be and W as first wall materials with sufficient low fuel retention for the deuterium-tritium (DT)-phase in ITER and shall, on the other hand, be used to develop and demonstrate ITER-compatible scenarios within the material limits. The identification of the source of impurities and the measurement of their radiation distribution in front of all plasma-facing components is of fundamental importance for the understanding of physical processes such as power exhaust, detachment, recombination, and recycling as well as of the erosion and redeposition properties.

A new endoscope with optimised divertor view has been developed for this study in order to survey and monitor the emission of specific impurities such as tungsten, beryllium, and the remaining carbon, if any, in the tungsten divertor of JET.

In May 2011, the endoscope was successfully installed on the torus. It has delivered from the very first JET pulse images of the emission of the selected transition lines.

II. DESIGN REQUIREMENTS

The endoscope must cover the spectral range from 390 nm to 2500 nm with a high optical transmittance ($\geq$30% in the designed wavelength range) as well as a high spatial resolution, that is $\leq$3 mm for the full depth of field ($\pm$0.7 m). The 3 mm in the object space corresponds to 0.067 mm in the image space at an optical system magnification of $\sim$45. The 50% modulation transfer function (MTF) spatial frequency in the image plane must be larger than 15 ℓ/mm (1.0/0.067). The endoscope field of view (FOV) must cover an angle of $\pm 8^\circ$ and the object distance is 4 m. The endoscope should

[a)]Invited paper, published as part of the Proceedings of the 19th Topical Conference on High-Temperature Plasma Diagnostics, Monterey, California, May 2012.

[b)]Author to whom correspondence should be addressed: Electronic mail: A.Huber@fz-juelich.de.

[c)]URL: www.fz-juelich.de/iek/iek-4.

[d)]See appendix of F. Romanelli *et al.*, Proc. 23rd IAEA Fusion Energy Conf. 2010, Daejon, Korea.

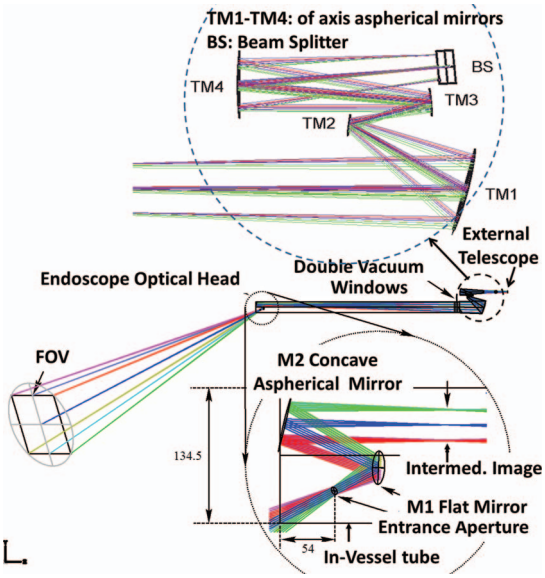

FIG. 1. Optical design overview.

be coupled to a set of four CCD cameras (two of them with micro-channel plate (MCP) image intensifiers) for scientific purposes and to two protection cameras in the infrared (IR) range. Each camera should have the same FOV. The endoscope should contain built-in hardware for *in situ* relative measurements of the transmission. The system shall be reasonably protected against coating of the first optics by impurities from the plasma. This can be achieved with a physical entrance pupil of diameter ≤ 8 mm. The system should able to operate in a strong magnetic field: up to B = 3.0 T toroidal magnetic field strength at the optical head, where the poloidal and radial field can change at a rate of 70 T/s and 20 T/s, respectively. The system must also withstand – without damage or loss of alignment – accelerations up to 7 g that can result from disruptions. The in-vessel tube and its in-vessel optical components must operate under vacuum conditions below 10^{-6} mbar and must be compatible with temperatures of 200 °C–350 °C.

III. OPTICAL DESIGN

The optical system has been designed with a field of view of 16°, viewing the divertor in both poloidal and toroidal directions. Figure 1 shows a schematic view of the endoscope optical design. The optical system consists of two main components: the endoscope optical head and the external telescope optical assembly. The optical head with entrance aperture and first mirrors is located in-vessel, i.e., in the vacuum, whereas the external telescope optical assembly is located outside the vessel. The main problem with refractive optical approaches is radiation damage: unhardened glass begins to show damage at 10^4 rad, fused silica, and glasses hardened with cerium oxide degrade 10%–20% at 10^7 rad.[2] Therefore, the design concept is based on reflective optics, mainly to be able to sustain high neutron radiation.

One of the objectives in the refinement of the new endoscope optical design is the optimization of the endoscope optical transmission. In this respect, it is favourable to minimize the overall number of optically active surfaces, in particular, elements inside the in-vessel tube, as it seems to be difficult to achieve highly reflective and low-scattering optical surfaces due to limitations in substrate and coating materials and in surface finishing processes. In the following, the number of surfaces in the endoscope internal head has been reduced to two mirrors while preserving the optical system performance. The function of the endoscope optical head is to collect light and to transfer an image of the FOV over a distance of ~2 m from the in-vessel optical aperture through the vacuum windows to the outside. There is an intermediate image plane, approximately at the interface between the endoscope head structure and the in-vessel tube, where a field stop has been positioned to block stray light. Figure 1 (bottom) shows also a schematic view of the endoscope head optical design from the entrance aperture to the field stop position. The optics consists of a plane mirror M1 and a concave aspherical mirror M2. The entrance aperture stop is circular with a diameter of 8 mm. The mirrors in the endoscope head are off axis and made from Al 6061 with an optical surface manufactured by single point diamond turning. The surface was left uncoated to mitigate a possible risk of degradation of the mirror coating in the in-vessel environment. The external telescope images the FOV, via the intermediate image generated by the endoscope head optics, onto the focal planes of the various camera systems. It consists of a four-mirror aspherical off axis arrangement (TM1–TM4) and a beam splitter unit, the first optical element of which is a reflective 50/50 beam splitter (BS). Figure 1 (top) shows a schematic overview of the external telescope. All mirrors TM1–TM4, including the BS, have been coated with Ag and a SiO_2 protection layer to enhance reflectivity especially in the visible (VIS) wavelength range.

The ghost reflections at the vacuum window interface and means how to mitigate them have been analysed. To mitigate the ghost reflections at the vacuum/air–glass interfaces, the vacuum windows have been coated by an anti-reflection (AR) layer. Additionally, we resorted to wedging of the windows. For a complete separation of the ghost images induced by the vacuum windows on the MCP, the required wedge angle would be at least 2°. AR-coatings allow mitigation down to a level of 0.04%–0.16% reflected power. Wedged vacuum windows in combination with a field stop aperture allow a complete elimination of ghost images induced by the windows.

IV. MECHANICAL CONSTRUCTION OF THE ENDOSCOPE

The endoscope is a prototype for testing an ITER relevant design concept based on reflective optics only. The diagnostic is located in octant 1, in a lower limiter guide tube (horizontal port at 330 mm below the equatorial plane). The mechanical layout concept of the endoscope system is presented in Fig. 2. The endoscope is formed by the in-vessel tube that holds the optical head with front mirrors. To keep the optical transmittance as high as possible, the number of first mirrors has been reduced to two. The materials of the mirrors and the structure are made of aluminium (AL6061), that is thermally treated forged material, in order to achieve a homogeneous thermal

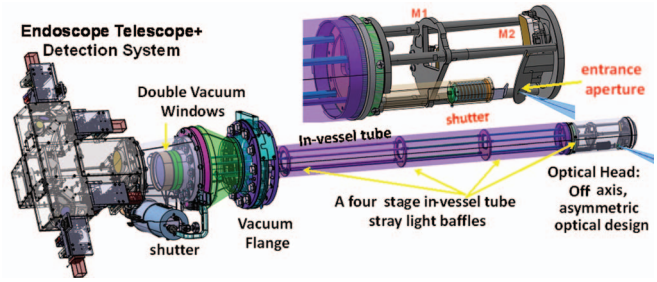

FIG. 2. Mechanical construction of the endoscope system.

behaviour. All mirrors are mounted "stress free" with a three point support allowing alignment within the structure.

The entrance aperture has been fixed to the optical head in order to serve as a stable aperture stop. The entrance aperture is chosen small, 8 mm in diameter, to prevent transmittance degradation with time due to impurity deposition and erosion by fast neutral particles as well as to fulfil the requirements for the depth of field (DOF). For an improved reduction of the stray light inside the in-vessel tube, four baffle apertures have been inserted in the beam path.

All optical components of the external telescope optical assembly as well as the detection system are located outside the vessel. The baseline design is a box-like structure with the four mirrors and 90° BS integrated with fixations to the vacuum flange. The box is closed by means of a sheet of aluminium without structural support in order to reduce the stress induced on the optical elements. As mentioned above, all external telescope mirrors TM1–TM4, including the BS, are made of aluminium, coated with Ag and a SiO_2 protection layer. The vacuum interface is based on the double vacuum windows that are the standard solution on JET used for tritium safety.

In this design we use fused silica, limiting thus the spectral measuring range to 2500 nm. An exchange of the windows to achieve sufficient transmittance in the far IR wavelength range (for example sapphire) is possible and could make such IR measurements possible. All mirrors have been manufactured by single point diamond turning procedures. The quality of all mirrors (the surface form errors and surface micro roughness) has been measured interferometrically by the mirror manufacturer. Table I gives an overview of the root mean square (RMS) surface form error and micro roughness Rq of the endoscope mirrors. All RMS deviations are below $\lambda/10$.

The new endoscope system provides information over a substantial portion of the toroidal extension of JET, i.e.,

TABLE I. Mirror RMS surface form error and micro roughness.

Mirror	Surface form error (RMS)	Surface micro roughness (Rq)
M1	17 nm	1.7 nm
M2	31 nm	...
TM1	40 nm	3.1 nm
TM2	16 nm	4.3 nm
TM3	51 nm	5.8 nm
TM4	43 nm	4.6 nm
BS	... / 24 nm	1.7 nm / 2.0 nm

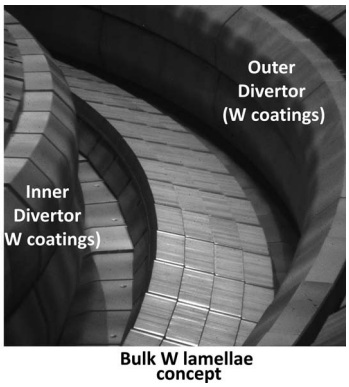

FIG. 3. The view through the endoscope into the Octant 2 divertor (from the Octant 1B lower limiter guide tube).

more than 1/8th–2/8th of the divertor. This large observation area avoids misinterpretation of measured data due to possible toroidal inhomogeneities. Figure 3 shows a view of the divertor recorded by the new device.

Plasma particles influence the surface of the first mirror by erosion and deposition. Additionally, glow discharge used during the JET wall conditioning can significantly damage the surface of the in-vessel mirrors. Beryllium evaporation would lead to formation of layers on the mirror surface too, which degrades the reflection coefficient significantly.

The entrance aperture of the KL11 endoscope is equipped with a mechanical shutter inside the JET vessel and operated in vacuum to minimise the degradation of the first mirror. Therefore, the shutter will be opened only before discharges where measurements are performed. The time response for shutter movement between open and close positions (and vice versa) is about 30 s.

The shutter system is operated pneumatically in a closed pressure circuit filled with neon to allow reliable function at all conditions at JET. In case of a leakage, the amount of released neon does not jeopardise the JET vacuum and the shutter moves to an open position per default to guarantee continuation of the measurements. The rear side of the shutter is polished and used as a mirror to perform *in situ* transmission measurements in closed position.

The principal setup of the shutter system is shown in Fig. 4. The pneumatic piston carrying the shutter is mounted

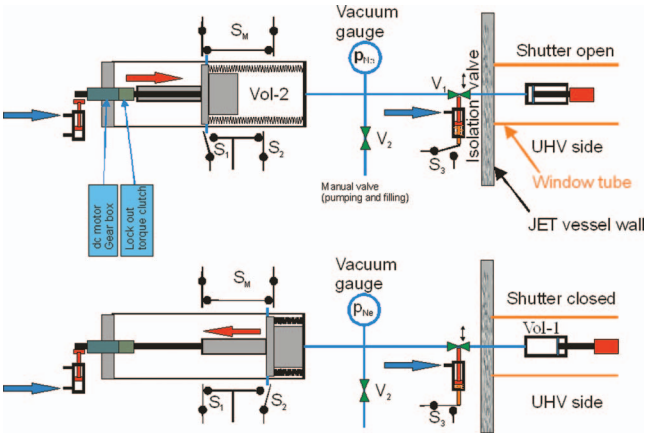

FIG. 4. Schematic diagram of KL11 shutter system (top: shutter open; bottom: shutter closed).

inside the endoscope head (see also Fig. 2). A tube inserted inside the endoscope connects the pressure volume Vol-1 with a larger volume Vol-2 outside the vessel. Vol-2 has the maximal value when the shutter is open and the neon gas pressure is about 0.2 bar. To close the shutter, the motor driven piston controlling Vol-2 is activated. Insertion the piston reduces Vol-2 and the pressure increases up to a factor of 20 to about 4.0 bar (displayed by the pressure gauge). At this pressure, the piston at Vol-1 moves forward by 18 mm and the shutter is closed. For re-opening, the movement of the piston in Vol-2 is inverted.

A finite element method (FEM) multi-physics calculation was performed including the preceding thermal and mechanical loads, to ensure that the endoscope shows no structural failure and that its performance is not affected. It revealed a thermal expansion of about 5 mm of the front head in the axial direction while it also permitted to find a resonance frequency of about 30 Hz, higher than the imposed lower limit of 14 Hz. On a more global point of view, the reserve factor of most components was kept higher than 5 even if it was a challenge to raise the RF of mirror M2 to about 1. Global static deformation of the endoscope is about 1.5 mm.

While concept and design were considered as partially validated by the global multi-physics analysis, certification and validation tests were anyway carried out. The most critical one has been without doubt the vibration test, which searched for the low resonance frequency between 0 and 50 Hz at 7 g in vertical direction and found it (for most directions and cases) around 20 Hz, a successful achievement over the 14 Hz specification. The endoscope also withstood the thermal baking test, which brought it to thermal conditions comparable to operation (absolute values and gradients). The endoscope showed high stability of the line of sight during this temperature cycling test. This stability in measurement despite environmental loading was the main validation step.

V. DETECTION SYSTEM

The endoscope is equipped with four digital CCD cameras: Allied Vision Technologies (AVT) Pike F-100B camera, 1000 × 1000 pixel, Pixel size: 7.4 μm × 7.4 μm, FireWire data connection via optical fibres, max. 33 fps at full resolution and 16 bits data output. Each camera is combined with a filter wheel for narrow band interference (with a ≈1.5 nm spectral bandwidth) and neutral density filters (see Fig. 5). Two of these cameras are equipped with MCP image intensifiers (Proxitronic BV2562BZ, photocathode Ø25 mm). The MCP image is transferred via a fibre optic taper to the CCD camera sensor. These cameras are foreseen for the measurements of the emission of spectral lines in the near ultraviolet (UV) and blue spectral range. Magnification of the taper is 25:11 to match the image on the MCP photocathode.

The two non-intensified cameras are equipped with the taper to keep the image size for all cameras the same. The sensor of each cameras is cooled by a thermoelectric Peltier module that draws heat away from the sensor resulting in the reduction of the dark current noise that accumulates during extended integration periods, thus enabling the camera to view a low contrast image in a low-light scene. But the main reason for the CCD camera cooling is the protection of the camera sensor against neutron radiation damage because the endoscope performance on JET must be unaffected by neutron fluxes of 10^{13}–10^{14} n^0 $m^{-2}s^{-1}$ (with a significant fraction at 14 MeV) and gamma rays. The cooler holds the CCD sensor temperature at −12 °C (with camera power switched on). The temperature of the sensor is monitored by PT100 Platinum resistance thermometers. After 7 months of operation on JET, we do not see any serious damage of the camera sensors.

Thus, these four digital CCD cameras provide two-dimensional images simultaneously for 4 different spectral lines: two in the near UV to blue spectral range and two in the red spectral range ($\lambda \geq 510$ nm). In addition, two protection cameras in the $\lambda \geq 0.95$ μm range have been integrated in the optical design for the real time wall protection during JET plasma operations. They are responsible for the identification of the hot spots as well as for the real time temperature measurements at hot spots and in general of other wall components. Each camera has the same complete FOV. To fulfil this requirement the 90°-BS has been located at the exit pupil (the entrance pupil is imaged onto the BS).

Figure 6 shows a schematic view of the beam splitter unit, with the 50/50 reflective beam splitter (90° beam splitter) in the centre, the dichroic beam splitters DCLP-510, the dichroic beam splitters DCSP-950 for the protection cameras, the mirror TM4, and the four scientific AVT camera assemblies. The full control of the detection system (control of the filter exchanger, camera cooling, sensor temperature monitoring) is based on the Simatic S7-PLC technique. The control of the detection system can be done by the operator from the JET control room.

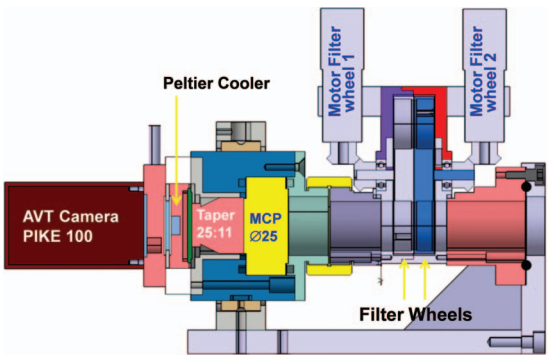

FIG. 5. Camera unit.

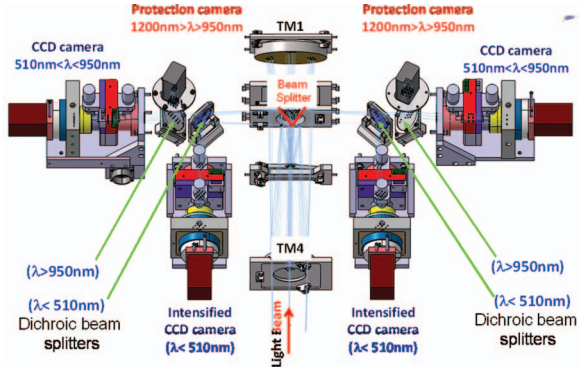

FIG. 6. Detection system.

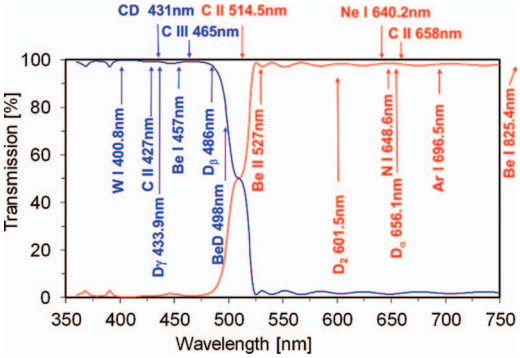

FIG. 7. The transmission characteristics for the dichroic beam splitters DCLP-510 with identification of the selected emission lines.

Figure 7 shows the transmission characteristics of the dichroic beam splitters DCLP-510 with identification of expected impurities lines. The detection system can thus fulfil the requirements of monitoring the impurity radiation of all species expected on JET with the ITER-like wall.

VI. PERFORMANCE

The spatial resolution of the designed endoscope shall be better than 3 mm at the object plane and the depth of field of the endoscope should be DOF $\geq$ 1440 mm.

For the optical performance tests and for the verification of the FOV a mock up of the JET divertor has been manufactured. The precise positioning of the endoscope and mock up divertor has been achieved with the help of photogrammetry. The MTF target has been located at distances of 5080 mm, 4720 mm, 4000 mm, 3640 mm, 3280 mm, and 2920 mm. The images of the divertor mock-up with MTF target have been taken by every camera and the MTF has been calculated. Figure 8 shows the measured MTF for one camera. The camera was focused onto the object plane at a distance of 3640 mm. The presented MTF represent the optical performance of the optical system of the endoscopes combined with the PIKE camera; accordingly, the performance of the optical system alone is better than the presented one. In the entire measured region between extremes, the MTFs show values larger than 50%. Thus the optical system fulfils completely the spatial resolution and DOF requirements.

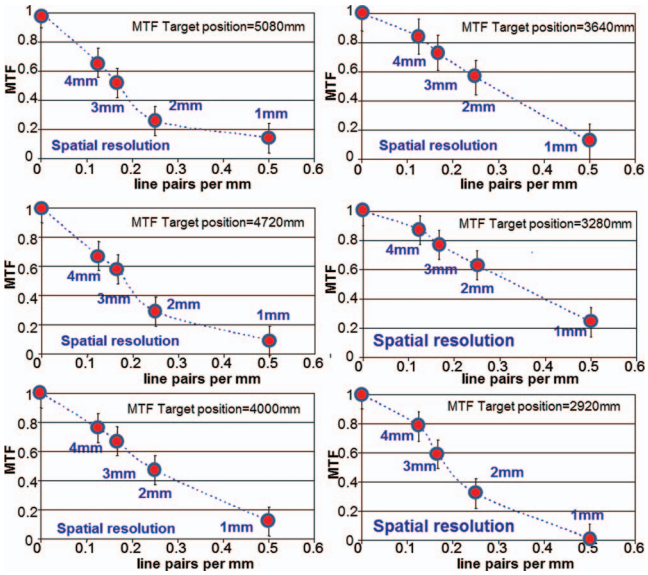

FIG. 8. The measured modulation transfer function (MTF), showing the contrast at various spatial frequencies at different distances from the entrance aperture.

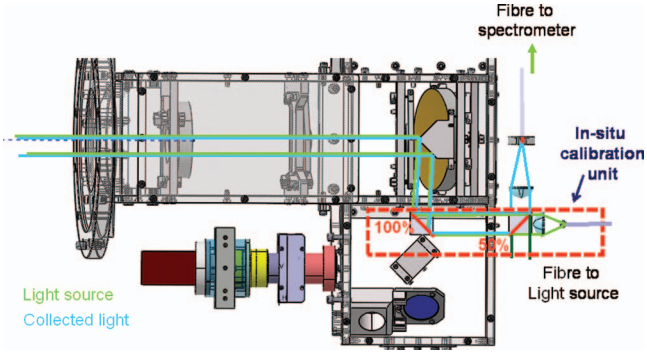

FIG. 9. *In situ* calibration unit.

The new optical design includes options for the *in situ* calibration of the endoscope transmittance during the experimental campaign, which allows a continuous tracing of possible transmittance degradation with time. The *in situ* calibration unit contains the light source and the detector (spectrometer) (see Fig. 9). The light is introduced into the endoscope optical system from the location of the camera and will be reflected from the rear side of the closed shutter (mirror surface) back to the detector. The first measurements (reference spectrum) were made with a combination of the *in situ* unit with an Ulbricht sphere. The following measurements should be compared with this reference spectrum. According to design requirements, the endoscope must cover the spectral range from 390 nm to 2500 nm with optical transmittance $\Im \geq 30\%$. Figure 10 shows the endoscope transmittance recorded directly after endoscope installation (reference transmittance) and the transmittance measured after 7 months of JET operation. The measured transmittance of the entire endoscope system for wavelengths $\lambda > 400$ nm meets the requirements completely. They are still met after 7 months for wavelengths $\lambda > 500$ nm. For $\lambda < 500$ nm we observe some degradation ($\Delta\Im \approx 40\%$ at 400 nm) assumably due to impurity deposition on the first mirror. To compensate the loss of transmittance at 400 nm, the camera sensors will be cooled

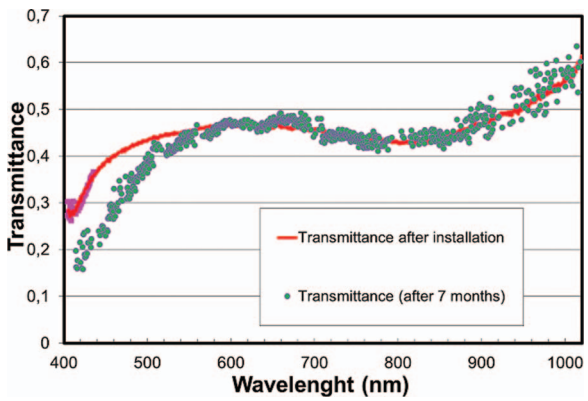

FIG. 10. The transmittance of the endoscope optical system.

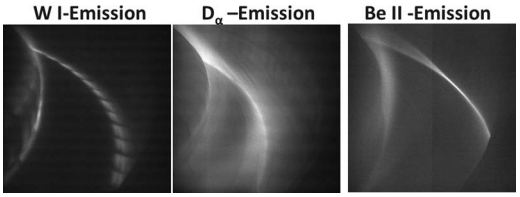

FIG. 11. W I-, D_α-, and Be II-emission profiles in the divertor region during the density limit experiment in JET.

to temperatures of about −10°C leading to a significant increase in the dynamical range of cameras. Thus, the cooled cameras can be operated at larger amplification of the image intensifiers.

VII. FIRST RESULTS WITH THE KL11 ENDOSCOPE SYSTEM

The installation of the ILW on JET during the last shutdown gives the opportunity to study tokamak operation with ITER relevant wall materials at densities close to the Greenwald limit. The operation at high density with a detached divertor is a key element of the current ITER design. Volume recombination in hydrogenic plasmas plays an important role in plasma detachment from the target plates of diverted discharges.[3,4] Experimental evidence of recombination has been obtained in JET from the increase in the ratio of the intensities of the Balmer series lines of excited hydrogen atoms, D_γ/D_α and D_β/D_α.[5,6] For characterisation of the plasma detachment processes, it is very important to determine the source of impurities and of their radiation distribution in front of all plasma-facing components as well as to determine which regions of the divertor are affected by recombination. The new endoscope, having an improved spatial resolution over previous designs and delivering images of high quality, gives a unique opportunity for monitoring the impurity radiation as well as the changes in the recombination region by simultaneous imaging of D_α, D_β, D_γ emission from the divertor with CCD cameras with the same FOV. Figure 11 shows the examples of the WI- (400.8 nm), D_α- (656.3 nm), and Be II- (527 nm) emission profiles taken during an ohmic density limit experiment with exposure times of 30 ms for WI and Be II lines and 0.1 ms for D_α. The image intensified camera which delivers the WI-emission profile was operated at the lowest MCP amplification and thus demonstrates the possibility to resolve the line radiation with respect to the optical transmittance in the UV range at 400 nm. Those images are then inverted by a singular value decomposition method,[7,8] to provide local emissivities. Figure 12 provides snapshots of the D_γ-emission (left) and D_γ/D_α ratio (right) in the divertor region for a L-mode density limit discharge ($B_T = 2.0$ T, $I_p = 2.0$ MA, ohmic). In both cases the inner divertor was detached. In Fig. 12 (upper row) detachment has just started in the outer divertor and the recombination is concentrated near the target plate. As the density is increased, the recombination region expands along flux surfaces away from the divertor plate towards the X-point (lower row). The radiation pattern shifts from the separatrix into the outer scrape-off layer and inside the separatrix to the vicinity of the X-point. The D_γ/D_α ratio, an indicator of the dominance of either excitation or recombination in determining the D_γ brightness, increases at least by a factor of two, which is attributed to the onset of recombination.

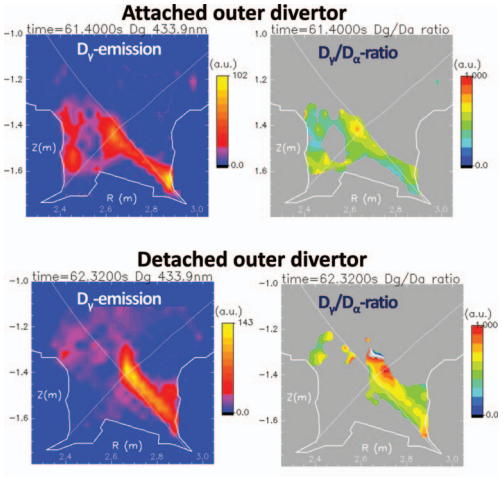

FIG. 12. Tomographic reconstructions of D_γ-emission (left column) and D_γ/D_α-ratios (right column) with attached (upper row) and detached (lower row) outer divertor.

VIII. CONCLUSION

The KL11 endoscope was successfully installed in May 2011, timely more than 2 months before JET restart. The information conveyed by all KL11 cameras over the expected toroidal extension of the JET divertor is fully consistent with the requested field of view. The spatial resolution of the optical system delivered the expected optical performance, which is better than 2 mm at the object plane and thus completely fulfils the requirement of a resolution ≤3 mm. The transmittance for wavelengths $\lambda > 500$ nm also meets the requirements completely. The endoscope delivers, from the first JET pulse after the EP2 restart on, images of the emitted radiation of the selected transition lines. The new endoscope has greatly improved the resolution and the quality of the images and of tomographic reconstruction of the poloidal distribution of radiation for different plasma species. The first results achieved by the endoscope have been presented and discussed.

ACKNOWLEDGMENTS

This work, supported by the European Communities under the contract of Association between the European Atomic Energy Community (EURATOM) and Forschungszentrum Jülich (FZJ), was carried out within the framework of the European Fusion Development Agreement. The views and opinions expressed herein do not necessarily reflect those of the European Commission.

[1]G. F. Matthews *et al.*, Phys. Scr. **T145**, 014001 (2011).
[2]S. S. Medley, Rev. Sci. Instrum. **70**, 794 (1999).
[3]D. Lumma, J. L. Terry, and B. Lipschultz, Phys. Plasmas **4**, 2555 (1997).
[4]S. I. Krasheninnikov, Phys. Plasmas **4**, 1638 (1997).
[5]A. Loarte, J. Nucl. Mater. **118**, 241–243 (1997).
[6]G. M. McCracken *et al.*, Nucl. Fusion **38**, 619 (1998).
[7]G. H. Golub and C. F. Van Loan, *Matrix Computation* (John Hopkins University, Baltimore, 1983).
[8]A. Huber *et al.*, J. Nucl. Mater. **925**, 313–316 (2003).